

# KPROJ: A Program for Unfolding Electronic and Phononic Bands

Jinxin Chen<sup>a</sup>, Mingxing Chen<sup>a,\*</sup>

<sup>a</sup>*School of Physics and Electronics, Hunan Normal University, Key Laboratory for Matter Microstructure and Function of Hunan Province, Key Laboratory of Low-Dimensional Quantum Structures and Quantum Control of Ministry of Education, Changsha 410081, China*

## ARTICLE INFO

### Keywords:

Band unfolding  
Layer projection  
Plane wave  
Phonon  
Lcao

## ABSTRACT

We introduce a program named KPROJ that unfolds the electronic and phononic band structure of materials modeled by supercells. The program is based on the  $k$ -projection method, which projects the wavefunction of the supercell onto the  $\mathbf{k}$ -points in the Brillouin zone of the artificial primitive cell. It allows for obtaining an effective "local" band structure by performing partial integration over the wavefunctions, e.g., the unfolded band structure with layer-projection for interfaces and the weighted band structure in the vacuum for slabs. The layer projection is accelerated by a scheme that combines the Fast Fourier Transform (FFT) and the inverse FFT algorithms. It is now interfaced with a few first-principles codes based on plane waves such as VASP, Quantum Espresso, and ABINIT. In addition, it also has interfaces with ABACUS, a first-principles simulation package based on numerical atomic basis sets, and PHONOPY, a program for phonon calculations.

### Program summary

Program Title: KPROJ  
Developer's repository link: <https://github.com/mxchen-2020/kproj>  
Licensing provisions: GPLv3.0  
Programming language: Fortran 90

### Nature of problem:

Supercells are widely used to model doped systems and interfaces within the framework of first-principles methods. However, the use of supercells causes band folding, which is unfavorable for understanding the effects of doping and interfacing on the band structure of materials. Moreover, the folding also brings difficulties in explaining the results of angle-resolved photoemission spectroscopy experiments.

### Solution method:


This program is designed to calculate the unfolded band structure for systems modeled by supercells. The unfolding is performed by projecting the wave functions of the supercell onto the  $\mathbf{k}$ -points in the BZ of the primitive cell. The projector operator is built by the translation operator and its irreducible representation. The layer-projected band structure is obtained by integrating the wavefunction in a selected spatial window, for which the FFT and inverse FFT algorithms are used to accelerate the calculation.

## 1. Introduction

First-principles methods based on the density-functional theory (DFT) have made great successes in calculating electronic structures of solid states. Within this framework, supercells are widely used to model doping and interface[1–11]. Unfortunately, the use of supercells leads to band folding, which hides the nature of the band structure. For instance, an indirect band gap may appear as a direct band gap when the valence band maximum (VBM) and conduction band minimum (CBM) located at different  $\mathbf{k}$ -points are folded to the same  $\mathbf{k}$ -point. As the size of the supercell becomes large, the calculated band structures may look completely different from that of the primitive cell. Such an effect is unfavorable for understanding the effects of chemical doping and interfacing on the band structure of materials. Moreover, the folded bands can cause troubles as one tries to explain the results of angle-resolved photoemission spectroscopy (ARPES)[12, 13] based on the calculated band structure. Therefore, it is necessary to eliminate the folded bands to facilitate the comparison between the DFT and ARPES results.

Over the past decades, many efforts have been devoted to developing band unfolding techniques. In the early 1980s, Weinert *et al*[14] obtained the unfolded band structure of  $\text{Cu}_3\text{Au}$  by projecting its wavefunctions from first-principles calculations onto the  $\mathbf{k}$ -points in the Brillouin zone (BZ) of the face-centered cubic primitive cell of Cu, which allows for understanding the effect of alloy on the band structure of Cu. Popescu *et al*[15, 16] proposed a similar method within the framework of plane waves, allowing for obtaining an effective band structure for random alloys modeled by large supercells. Then, its formalism in the tight binding approximation based on atomic orbitals[17–19] and Wannier functions[20] was also built. So far, several programs have been developed for the band unfolding based on the above-proposed methods[21–29].

In this communication, we introduce a band unfolding program named KPROJ based on the  $k$ -projection method[30], which uses the projector built by the translation operator and its irreducible representation. One prominent feature of the program is that it allows for calculating the weights of projected wavefunctions in an artificially defined spatial window. This functionality is ideally suited for interfaces and systems modeled by slabs, for which a layer projection may be needed to extract an effective unfolded band

 [mxchen@hunnu.edu.cn](mailto:mxchen@hunnu.edu.cn) (M. Chen)

ORCID(s): 0000-0002-5779-3369 (M. Chen)

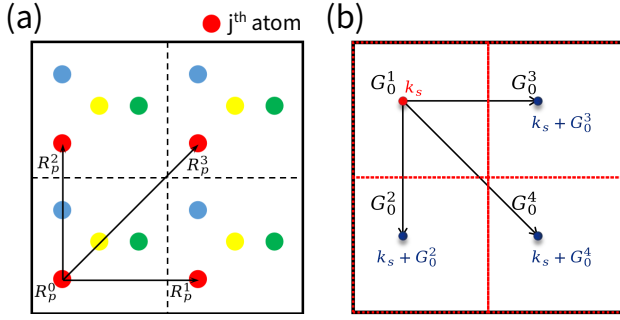


**Fig. 1:** Translation vectors in the real and reciprocal spaces. (a)  $R_p^M$  in real space for a  $2 \times 2$  square lattice supercell. (b) Corresponding  $G_0^s$  in the reciprocal space.

structure for the component systems. An algorithm combining the FFT and back FFT is used to accelerate the layer projection. It is now interfaced with a few ab initio packages such as VASP[31–33], Quantum Espresso[34], ABINIT[35], and ABACUS[36]. Besides, it also has interfaces to Phonopy[37].

## 2. The $k$ -projection method

The details of the  $k$ -projection method have been given in Ref. [30]. Here we give a brief description of its formalism. Assuming the lattice vectors of a supercell ( $A_i$ ) and the corresponding primitive cell ( $a_i$ ) are related by

$$\begin{pmatrix} A_1 \\ A_2 \\ A_3 \end{pmatrix} = \mathbf{M} \begin{pmatrix} a_1 \\ a_2 \\ a_3 \end{pmatrix} = \begin{pmatrix} M_{11} & M_{12} & M_{13} \\ M_{21} & M_{22} & M_{23} \\ M_{31} & M_{32} & M_{33} \end{pmatrix} \begin{pmatrix} a_1 \\ a_2 \\ a_3 \end{pmatrix}, \quad (1)$$

where  $\mathbf{M}$  is the transformation matrix between the lattice vectors of the supercell and the primitive cell. Here,  $\det \mathbf{M} = N_c$ , where  $N_c$  is the number of the unit cell. It means that there are  $N_c$  translation vectors ( $R_p^M$ ) of the primitive used to obtain a supercell. Fig. 1(a) shows  $R_p^M$  for a  $2 \times 2$  supercell of the two-dimensional (2D) square lattice.

One can also use the matrix  $\mathbf{M}$  to build the relation between their reciprocal lattice vectors. In the reciprocal space, multiple  $\mathbf{k}$ -points ( $\mathbf{k}_p$ ) in the first BZ of the primitive cell fold back to a single  $\mathbf{k}$ -point ( $\mathbf{k}_s$ ) in the first BZ of the supercell

$$\mathbf{k}_p = \mathbf{k}_s + \mathbf{G}_0^s, \quad (2)$$

where  $\mathbf{G}_0^s$  are the reciprocal lattice vectors of the supercell that map the folding. The number of  $\mathbf{G}_0^s$  equals to  $N_c$ . Fig. 1(b) schematically illustrates the folding in a  $2 \times 2$  supercell of the 2D square lattice. The scheme of the  $k$ -projection band unfolding technique is to build a projector operator ( $\hat{P}_{\mathbf{k}}$ ) based on the translation operators ( $\hat{T}_i$ ) and the irreducible representations ( $\chi_{\mathbf{k}_p}$ ) labeled by  $\mathbf{k}$  within the first BZ of the primitive cell and apply it to the wavefunctions of the supercell. Then, one needs to calculate the weights of the

projected wavefunctions

$$\hat{P}_{\mathbf{k}} = \frac{1}{h} \sum_i \chi_{\mathbf{k}}^*(i) \hat{T}_i \quad (3)$$

$$\psi_{\mathbf{k}_p} = \hat{P}_{\mathbf{k}_p} \psi_{\mathbf{k}_s}. \quad (4)$$

For wavefunctions expanded in plane waves, the weights of the projected wavefunctions for one of  $k_p$  corresponding to a  $\mathbf{G}_0^s$  are

$$W_{\mathbf{k}_s} = \langle \psi_{\mathbf{k}_p} | \psi_{\mathbf{k}_p} \rangle = \sum_{\mathbf{G}} |C_{\mathbf{k}_s}^{\mathbf{G}}|^2, \quad (5)$$

where  $\mathbf{G}$  satisfies

$$\begin{aligned} \mathbf{G} &= \sum_i M_i \mathbf{B}_i = \sum_j \left( \sum_i M_i (\mathbf{B}_i \cdot \mathbf{a}_j) \right) \mathbf{b}_j \\ &= \mathbf{G} + \mathbf{G}_0^s \end{aligned}$$

In the linear combination of atomic orbital approximation, the weights are in the form of

$$W_{\mathbf{k}_p} = \frac{1}{N_c} \left| \sum_M C_{\mathbf{k}_s, i, \alpha}^M e^{i\mathbf{k}_s \cdot \mathbf{R}_p^M} \right|^2 \quad (6)$$

where  $i\alpha$  index the orbital  $v$  of  $j$ -th atom,  $C_{\mathbf{k}_s, i, \alpha}$  were the calculated coefficient of corresponding atomic orbital.

For phonon calculations, the weights are

$$W_{\mathbf{q}_p} = \frac{1}{N_c} \sum_{\mathbf{R}_p^M} \sum_{\alpha\beta} C_{\alpha j}^* C_{\beta j'} e^{i\mathbf{q}_s \cdot \mathbf{R}_p^M} \delta_{\alpha\beta} \delta_{jj'} \quad (7)$$

where  $\alpha$  and  $\beta$  represent different directions of  $j$ -th atom.

For interfaces, the two components may be in different supercells. Therefore, one has to project the wavefunctions of the supercell onto appropriate  $k$ -points in the first BZ of the interested system. The effective unfolded band structure for the target component can be obtained by a layer projection, for which an integral over the projected wavefunction in a specified spatial window is performed, that is

$$A_{\mathbf{k}_p} = \int_{z_1}^{z_2} \psi_{\mathbf{k}_p}^* \psi_{\mathbf{k}_p} dr \quad (8)$$

We use an algorithm that combines FFT and the inverse FFT to accelerate the above calculations.

## 3. Description of the KPROJ program

### 3.1. Framework of the code

The above formalism is implemented in the KPROJ program, available at Github (<https://github.com/mxchen-2020/kproj>). The source code is written by Fortran90, for which: (i) main.f controls the workflow of the whole program; (ii) input.f reads the input parameters; (iii) mod\_wave.f reads the wave function; (iv) mod\_kproj.f performs band unfolding and layer projection calculation; (v) out\_bands.f outputs the

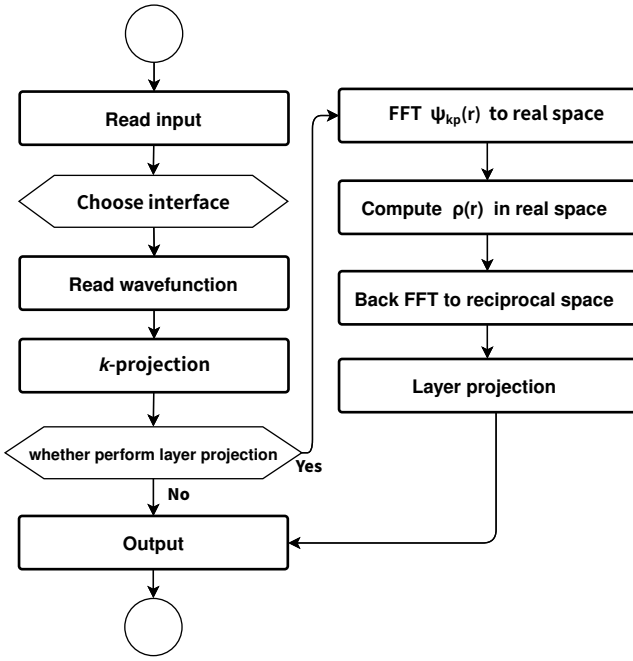


Fig. 2: Work flow of KPROJ.

**Table 1**  
Required input files for different interfaces

Interface	Input file(s)	Wavefunction
VASP	INKPROJ	WAVECAR
Quantum Espresso	INKPROJ	WFC_i.dat
ABINIT	INKPROJ	WFCAB
Phonopy	INKPROJ	band.yaml
ABACUS	INKPROJ	LOWF_K_i.dat pos_map.dat

weights of  $k$ -projected wavefunctions. Because the parameters for the wavefunction generated by Quantum Espresso are stored in the XML format, one has to install the XML library, which can be done by the terminal command "*make fox*". The executable file of KRPOJ can be obtained after compiling using "*make*". The workflow of KPROJ is shown in FIG. 2.

### 3.2. Inputs and outputs

The KPROJ program requires a few input files for different interfaces, which are listed in Table 1.

### 3.3. INKPROJ

INKPROJ provides the basic input parameters for band unfolding calculations. The detailed descriptions of the parameters are listed in Table 1, and a simple example is given in FIG. 3. A more detailed description of the input parameters can be found in the *doc* folder of the package.

### 3.4. pos\_map.dat

The file *pos\_map.dat* is only used for the LCAO methods. It stores the lattice vectors  $a_i$  of the primitive cell,

```

!transformation matrix from PC to SC in the real space
MAT_P2S = 5 0 0 \
           0 5 0 \
           0 0 1
LZLAYER = .TRUE. ! layer projection
zlay1 = 0.4
zlay2 = 0.6

LSORBIT = .FALSE. ! SOC
LCAO_UNFOLD = .FALSE. ! interface to abacus
Phonon_UNFOLD = .FALSE. ! interface to phonopy
#WFCAB = !interface to abinit, filename of wavefunction
  
```

Fig. 3: An example of the input file INKPROJ for the KPROJ.

```

1.0000000000000000 : lattice constant
3.79009234715989   0.0000000000000000   0.0000000000000000 } Lattice vectors
1.89504617357995   3.282316255329460   0.0000000000000000 } of primitive cell
0.0000000000000000   0.0000000000000000   41.77706547856130 }
3 0 0 }
0 3 0 } Transform matrix M
0 0 1 }
0 0 0 }
1 0 0 }
2 0 0 }
0 1 0 }
1 1 0 } 1th Atom and its RpM
2 1 0 }
0 2 0 }
1 2 0 }
2 2 0 }
0 0 0 }
1 0 0 }
2 0 0 }
0 1 0 }
1 1 0 } 2th Atom and its RpM
2 1 0 }
0 2 0 }
1 2 0 }
2 2 0 }
0 0 0 }
1 0 0 }
2 0 0 }
0 1 0 }
1 1 0 } 3th Atom and its RpM
2 1 0 }
0 2 0 }
1 2 0 }
2 2 0 }
.....
  
```

Fig. 4: The *pos\_map.dat* for  $3 \times 3$  silicene. The equivalent atoms are placed together and the  $R_p^M$  are given.

the transformation matrix  $M$ , and corresponding translation vectors  $R_p^M$  from the primitive cell to the supercell. Fig.1 shows an example for a  $3 \times 3$  supercell of silicene. We provide a program called "*supercell*" in the folder *utils* to help users generate supercells and the file *pos\_map.dat*.

### 3.5. Output files

The KPROJ package has two output files. One is a log file named OUTKPROJ. The other one is *bs\_projected.dat*, which stores energy eigenvalues and the calculated weights of the  $k$ -projected wavefunctions. We provide a post-processing program called *futils*, which uses *bs\_projected.dat* to prepare files for plotting in formats such as *xmgrace*, *gnuplot* and *opendx*.

### 3.6. Utilities

There are a few utilities that can facilitate the use of KPROJ.

(i) *supercell* is a program for generating supercells and the

file `pos_map.dat`. Users are only required to provide the transformation matrix  $M$  in Eq. (1). It is under the directory `Utils` and the executable file can be obtained after `make`.

(ii) `kpts_path` is under the directory of `Utils/supercell` and used to generate the  $k$ -points along a high symmetry line defined by two  $k$ -points, i.e.,  $K_i$  and  $K_f$ , which are in the direct coordinate.

(iii) `ksplit` is designed to split the  $k$ -points in a KPOINTS file into a few files named `KPOINTS_i`, which can be used for heavy calculations.

(iv) `mergefile` combines several `bs_projected.dat` files named `bs_projected.dat_i` into one file. Note that the ordering should be consistent with the  $k$ -points in KPOINTS. It is under the directory of `src`, which can be obtained by `make mergefile`.

(v) `futils` prepares files for plotting using the obtained `bs_projected.dat`, which can be obtained by `make futils` under the directory `src`.

## 4. Applications

Below we show a few applications of the code in revealing the effects of doping and interfacing on the band structures of materials.

### 4.1. Graphene supercells

We start with perfect graphene in a  $\sqrt{7} \times \sqrt{7}$  supercell. Fig.5(a) and (b) depict the geometric structure and fig.5(b) shows the BZs of the primitive cell and supercell. Fig.5(c) shows the band structure along the high symmetry lines in the BZ of the primitive cell directly obtained from standard DFT calculations. One can see that the band structure of the supercell shows similarity to the one for the primitive cell only near K due to the existence of band crossing. However, the features near  $\Gamma$  and M are distinctly different. The unfolded band structure shown in Fig. 5(d) agrees with the one calculated using the primitive cell.

### 4.2. Defected graphene

Doping and defects play an important role in tuning the electronic properties of materials[38–43]. Within the framework of first-principles calculations, such systems are usually modeled by supercells. Fig. 6(a) shows the geometric structure of defected graphene derived from a  $5 \times 5$  supercell, for which the BZ is shown in Fig. 6(b). Fig. 6(c) shows the band structure for the defected  $5 \times 5$  graphene. It looks completely different from the band structure of the perfect graphene. In addition, there are two new features. One is that there are dispersionless bands near the Fermi level. The other one is that there is no longer a gapless Dirac cone at K. Instead, it has a band gap. By projecting the wavefunctions of the defected graphene onto the  $k$ -points in the first BZ of the corresponding primitive cell, the dispersionless bands are gone and a band gap in the Dirac cone at K can be seen. Moreover, there are minigaps in the electronic bands. This effect is due to the perturbation of the defects.

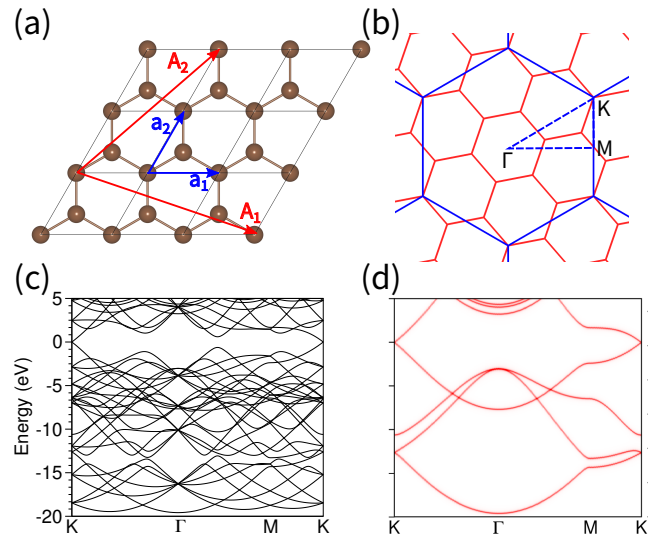


**Fig. 5:**  $k$ -projected (unfolded) band structure for perfect graphene. (a) Geometric structure of graphene in a  $\sqrt{7} \times \sqrt{7}$  supercell. The lattice vectors of the primitive cell and the supercell are shown in blue and red, respectively. (b) The first BZs of the primitive cell (blue hexagon) and the  $\sqrt{7} \times \sqrt{7}$  supercell (red hexagons). High symmetry points are labeled. (c, d) The band structures without and with band unfolding along the dashed lines shown in (b).

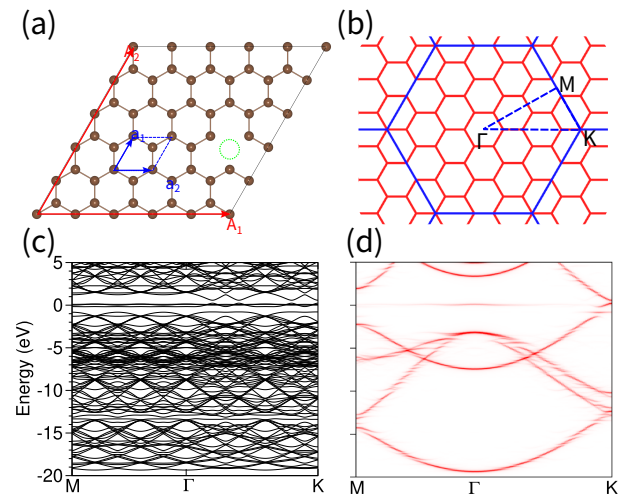


**Fig. 6:**  $k$ -projected band structure for defected graphene. (a) Top view of the structure with one defect in a  $5 \times 5$  supercell. (b) The first BZs of the primitive cell (blue) and the supercell (red). High symmetry lines are shown in blue dashed lines. (c, d) respectively show the band structures without and with band unfoldings.

### 4.3. Graphene bilayer on 6H-SiC

Now we show an application of KPROJ in interfaces. We performed calculations for a graphene bilayer (graphene-2L) on 6H-SiC(0001), which has two types of terminations, i.e., Si and C terminations[44–51]. Here, we consider an interface structure consisting of a  $2 \times 2$  supercell of the

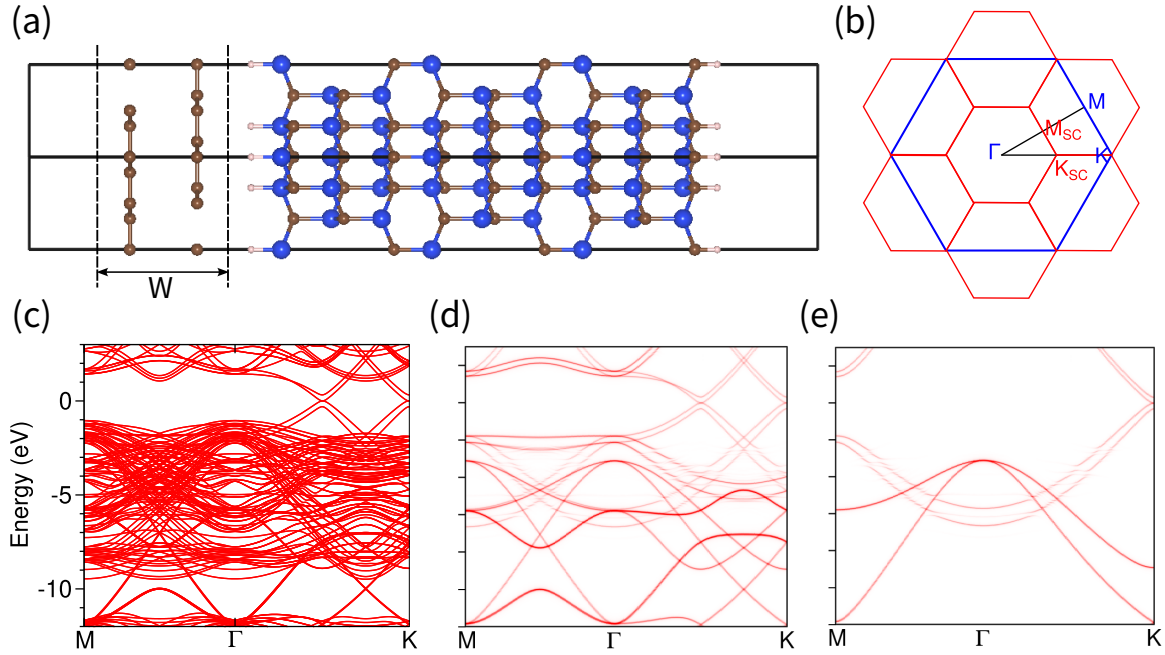


**Fig. 7:**  $k$ -projected band structure for graphene-2L/6H-SiC(0001). (a) Geometric structure of the interface structure. The wavefunctions in the spatial window defined by  $W$  are selected for the  $k$ -projection calculations for graphene-2L. (b) The first BZ of graphene-2L/6H-SiC(0001) and the primitive cell of graphene. The high symmetry points and lines used for the calculations are shown. (c) The band structure obtained from a standard VASP calculation. (d) The band structure weighted by contributions of the graphene-2L. (e) The  $k$ -projected band structure for the graphene-2L.

graphene-2L on a  $\sqrt{3} \times \sqrt{3}$  Si-terminated 6H-SiC(0001), which is saturated by hydrogen atoms. The geometric structure is shown in Fig. 7(a), for which the BZs are shown in Fig. 7(b). The calculated bands along the BZ of the graphene primitive cell are shown in Fig. 7(c). Note that there are two sets of band-crossing along the path from  $\Gamma$ -K. One is located at a  $\mathbf{k}$ -point (named  $k_q$ ) in the middle of  $\Gamma$ -K and the other emerges at K. The extra band-crossing at  $k_q$  is due to band folding, which still exists in the band structure weighted by the contribution of graphene shown in Fig. 7(d). Then, we perform  $k$ -projection over the wavefunctions in the overlayer. The wavefunctions in the spatial window defined in Fig. 7(a) are chosen for the calculations. Then one can obtain an "effective" band structure for the bilayer graphene. This main profile of the unfolded band structure shows great similarity with that of the freestanding systems, except for minigaps in the electronic bands. Therefore, one can deduce that the Si-terminated 6H-SiC(0001) with H-saturation has a minor effect on the band structure of the overlayer.

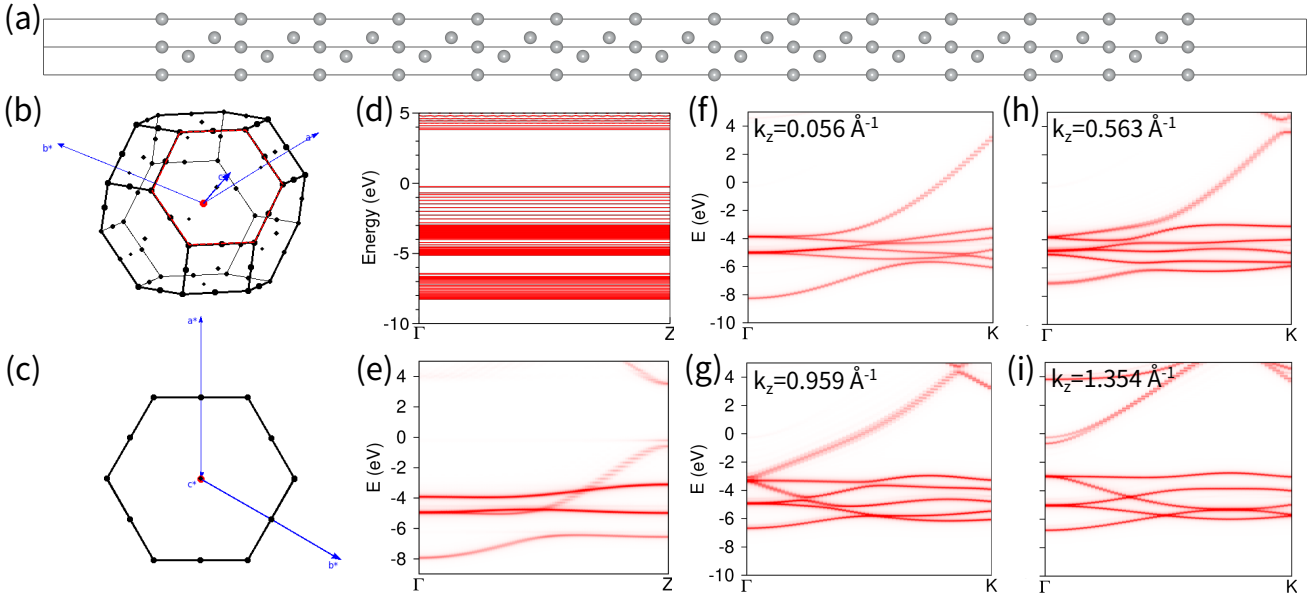
#### 4.4. Bulk projection of surfaces

Figure 8 shows the calculation for Ag(111). We build a slab with a thickness of 113 Å, which has 48 unit cells of Ag(111) along  $z$  [Fig 8(a)]. We then remove two Ag(111) layers from each side of the slab to make a surface structure. By calculating the dispersions along  $\Gamma - z$ , one obtains

dispersionless electronic bands [see fig. 8(d)]. By projecting the wavefunctions onto the  $\mathbf{k}$ -points in the BZ of the primitive cell of Ag bulk [Fig. 8(e)], one can obtain a band structure pretty much similar to that for the bulk phase. Note that the band crossing the Fermi level gets broadened as the energy goes to high energies, for which the surface effect plays a role. One can conveniently investigate the  $k_z$  dependence of the band structure for the slab by projecting its wavefunctions onto the  $k$ -points in the BZ of the Ag bulk. The unfolded bands with different  $k_z$ s were shown in fig 8(f-i).

#### 4.5. Phonons of defected graphene and moiré superlattices

Our KPROJ program also allows for unfolding phonon dispersions for doped materials and interfaces. We now show its application in the defected graphene and moiré superlattice with a twist angle of  $9^\circ$ . We use the small displacement method implemented in PHONOPY to obtain the phonon dispersions. The atomic forces induced by the displaced atom are calculated using LAMMPS[52] with a machine learning potential[53–58], which was also used for the geometric relaxation. To facilitate comparison, fig. 9(a) shows the phonon spectrum for the graphene primitive cell. Figs. 9(b) and (c) show the folded and unfolded phonon spectrums for the defected graphene discussed in subsection 4.2.



**Fig. 8:**  $k$ -projected band structure for Ag(111) slab. (a) Geometric structure of the Ag(111) slab. (b,c) The first BZs of bulk Ag and Ag(111) slab. (d) The band structures along  $\Gamma - z$ . (e) The band structure by projecting the wavefunctions of the slab onto the  $k$ -points in the BZ of the primitive cell of Ag bulk. (f-i) The  $k_z$ -dependence of the band structure with bulk projection.

The unfolded phonon dispersions overall look very much similar to those for the free-standing graphene. However, one can also see many minigaps, which is due to the effects of carbon defects.

We also performed layer  $k$ -projection for graphene moiré superlattice, that is, we project the eigenvectors contributed by the top layer onto the  $q$ -point in the BZ of the graphene primitive cell. The results are shown in fig. 9(d). A comparison with fig. 9(c) reveals that the twisting and stacking have a much weaker effect than defects on the phonon dispersions of graphene.

## 5. Conclusion

In this communication, we introduce our band unfolding program KPROJ, which allows for unfolding electronic and phononic bands of materials modeled by supercells. It is interfaced with popular DFT packages and PHONONPY. The code is user-friendly and is ideal for investigating interfaces due to a highly efficient algorithm for layer projection over wavefunctions in a selected spatial window. Moreover, a few utilities are provided to prepare the inputs and post-processing. We have demonstrated its applications in defected graphene and heterostructures of graphene, which allows for the revealing of the effects of defect and interface on electronic and phononic dispersions. Moreover, it is useful to interface the program with the codes based on the deep learning density functional theory Hamiltonian, which allows for investigating the effects of doping and interfaces on the band structure of large systems [59].

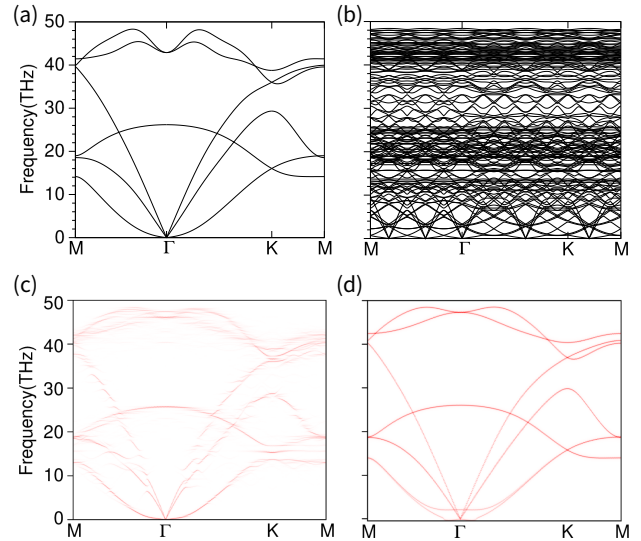


**Fig. 9:** Unfolded phonon dispersions for the defected  $5 \times 5$  graphene and a graphene moiré superlattice. (a) The phonon spectrum of graphene in the primitive cell. (b,c) The phonon dispersions for the defected graphene without and with band unfolding. (d) Unfolded phonon band structure with layer projection for graphene bilayer with a twist angle of  $9^\circ$ .

## 6. Acknowledgement

This work was supported by the National Natural Science Foundation of China (Grant No. 12174098).

## References

- [1] D. Radevych, M. Gajdardziska-Josifovska, C.J. Hirschmugl, M.A. Schofield, and M. Weinert.  $\beta$ -graphene monoxide: Two-dimensional

- crystal form of carbon monoxide. *Physical Review Materials*, 6(7):074006, 2022.
- [2] Z.Y. Zhu, X.F. Chen, W.B. Li, and J.S. Qi. Electric field control of the semiconductor-metal transition in two dimensional cuinp2s6/germanene van der waals heterostructure. *Applied Physics Letters*, 114(22), 2019.
  - [3] M. Ge, H. Wang, J.Z. Wu, C. Si, J.F. Zhang, and S.B. Zhang. Enhanced valley splitting of wse2 in twisted van der waals wse2/cr13 heterostructures. *npj Computational Materials*, 8(1):32, 2022.
  - [4] X.Y. Wei, J.Y. Zhang, B. Zhao, and Y.Z. Yang. Coexistence of valley polarization and chern insulating states in mos2 monolayers with np codoping. *Scientific Reports*, 10(1):9851, 2020.
  - [5] A. Grubišić-Čabo, J.C. Kotsakidis, Y.F., A. Tadich, M. Haldon, S. Solar, I. D. Bernardo, K.M. Daniels, J. Riley, E. Huwald, et al. Magnesium-intercalated graphene on sic: Highly n-doped air-stable bilayer graphene at extreme displacement fields. *Applied Surface Science*, 541:148612, 2021.
  - [6] B. Li, Z. Wan, C. Wang, P. Chen, B. Huang, X. Cheng, Q. Qian, J. Li, Z.W. Zhang, G.Z. Sun, et al. Van der waals epitaxial growth of air-stable crse2 nanosheets with thickness-tunable magnetic order. *Nature Materials*, 20(6):818–825, 2021.
  - [7] A.M. Holmes, S. Pakniyat, S.H. Gangaraj, F. Monticone, M. Weinert, and G.W. Hanson. Exchange splitting and exchange-induced non-reciprocal photonic behavior of graphene in cr i 3-graphene van der waals heterostructures. *Physical Review B*, 102(7):075435, 2020.
  - [8] Z.P. Sun, C.Q. Hua, X.L. Liu, Z.T. Liu, M. Ye, S. Qiao, Z.H. Liu, J.S. Liu, Y.F. Guo, Y.H. Lu, et al. Direct observation of sixfold exotic fermions in the pyrite-structured topological semimetal pdsb 2. *Physical Review B*, 101(15):155114, 2020.
  - [9] L. Yin, T. Berlijn, R. Juneja, L. Lindsay, and D.S. Parker. Competing magnetic and nonmagnetic states in monolayer vse 2 with charge density wave. *Physical Review B*, 106(8):085117, 2022.
  - [10] M. Bonilla, S. Kolekar, Y.J. Ma, H.C. Diaz, V. Kalappattil, R. Das, T. Eggers, H.R. Gutierrez, M.M. Phan, and M. Batzill. Strong room-temperature ferromagnetism in vse2 monolayers on van der waals substrates. *Nature nanotechnology*, 13(4):289–293, 2018.
  - [11] P. Chen, W.W. Pai, Y.H. Chan, V. Madhavan, M.Y. Chou, S.K. Mo, A.V. Fedorov, and T.C. Chiang. Unique gap structure and symmetry of the charge density wave in single-layer vse 2. *Physical review letters*, 121(19):196402, 2018.
  - [12] M.X. Chen, Z.Z. Ge, Y.Y. Li, D.F. Agterberg, L. Li, and M. Weinert. Effects of interface oxygen vacancies on electronic bands of fese/srtio 3 (001). *Physical Review B*, 94(24):245139, 2016.
  - [13] M.X. Chen, W. Chen, Z.Y. Zhang, and M. Weinert. Effects of magnetic dopants in (li 0.8 m 0.2 oh) fese (m= fe, mn, co): Density functional theory study using a band unfolding technique. *Physical Review B*, 96(24):245111, 2017.
  - [14] J.W. Davenport, R.E. Watson, and M. Weinert. Linear augmented-slater-type-orbital method for electronic-structure calculations. *v. spin-orbit splitting in cu 3 au. Physical Review B*, 37(17):9985, 1988.
  - [15] P. Voicu and Z. Alex. Extracting e versus k effective band structure from supercell calculations on alloys and impurities. *Physical Review B—Condensed Matter and Materials Physics*, 85(8):085201, 2012.
  - [16] P. Voicu and Z. Alex. Effective band structure of random alloys. *Physical review letters*, 104(23):236403, 2010.
  - [17] Z.J. Dai, G. Jin, and L.X. He. First-principles calculations of the surface states of doped and alloyed topological materials via band unfolding method. *Computational Materials Science*, 213:111656, 2022.
  - [18] C.C. Lee, Y.T. Yukiko, and O. Taisuke. Unfolding method for first-principles lcao electronic structure calculations. *Journal of Physics: Condensed Matter*, 25(34):345501, 2013.
  - [19] G.S. Mayo, Y. Felix, and J.M. Soler. Band unfolding made simple. *Journal of Physics: Condensed Matter*, 32(20):205902, 2020.
  - [20] K. Wei, B. Tom, and L.C. Cheng. Unfolding first-principles band structures. *Physical review letters*, 104(21):216401, 2010.
  - [21] M. Paulo VC, S. Sven, and B. Jonas. Effects of extrinsic and intrinsic perturbations on the electronic structure of graphene: Retaining an effective primitive cell band structure by band unfolding. *Physical Review B*, 89(4):041407, 2014.
  - [22] F.W. Zheng, P. Zhang, and W.H. Duan. Quantum unfolding: A program for unfolding electronic energy bands of materials. *Computer Physics Communications*, 189:213–219, 2015.
  - [23] T. Milan, J. Harald O, and V. Roser. Unfolding of electronic structure through induced representations of space groups: Application to fe-based superconductors. *Physical Review B*, 90(19):195121, 2014.
  - [24] Y.H. Tan, F.W. Chen, and A.W. Ghosh. First principles study and empirical parametrization of twisted bilayer mos2 based on band-unfolding. *Applied Physics Letters*, 109(10), 2016.
  - [25] F.W. Zheng and P. Zhang. Phonon unfolding: A program for unfolding phonon dispersions of materials. *Computer Physics Communications*, 210:139–144, 2017.
  - [26] I. Yuji, C. Abel, S. Atsuto, T. Atsushi, and T. Isao. Mode decomposition based on crystallographic symmetry in the band-unfolding method. *Physical Review B*, 95(2):024305, 2017.
  - [27] M.P. VC, T. Stepan S, S. Sven, and B. Jonas. Unfolding spinor wave functions and expectation values of general operators: Introducing the unfolding-density operator. *Physical Review B*, 91(4):041116, 2015.
  - [28] Uthpala Herath, Pedram Tavazde, Xu He, Eric Bousquet, Sobhit Singh, Francisco Muñoz, and Aldo H Romero. Pyprocar: A python library for electronic structure pre/post-processing. *Computer Physics Communications*, 251:107080.
  - [29] O. Rubel, A. Bokhanchuk, S.J. Ahmed, and E. Assmann. Unfolding the band structure of disordered solids: From bound states to high-mobility kane fermions. *Physical Review B*, 90(11):115202, 2014.
  - [30] M.X. Chen and M. Weinert. Layer k-projection and unfolding electronic bands at interfaces. *Physical Review B*, 98(24):245421, 2018.
  - [31] K. Georg and H. Jürgen. Ab initio molecular dynamics for liquid metals. *Physical review B*, 47(1):558, 1993.
  - [32] K. Georg and F. Jürgen. Efficiency of ab-initio total energy calculations for metals and semiconductors using a plane-wave basis set. *Computational materials science*, 6(1):15–50, 1996.
  - [33] K. Georg and F. Jürgen. Efficient iterative schemes for ab initio total-energy calculations using a plane-wave basis set. *Physical review B*, 54(16):11169, 1996.
  - [34] G. Paolo, A. Oliviero, B. Thomas, B. Oana, N. M. Buongiorno, C. Matteo, C. Roberto, C. Carlo, C. Davide, C. Matteo, et al. Advanced capabilities for materials modelling with quantum espresso. *Journal of physics: Condensed matter*, 29(46):465901, 2017.
  - [35] G. Xavier, A. Bernard, P.M. Anglade, J.M. Beuken, B. François, B. Paul, B. Fabien, C. Damien, C. Razvan, C. Michel, et al. Abinit: First-principles approach to material and nanosystem properties. *Computer Physics Communications*, 180(12):2582–2615, 2009.
  - [36] D.Y. Zheng, X.G. Ren, and L.X. He. Accurate stress calculations based on numerical atomic orbital bases: Implementation and benchmarks. *Computer Physics Communications*, 267:108043, 2021.
  - [37] T. Atsushi, C. Laurent, T. Terumasa, and T. Isao. Implementation strategies in phonopy and phono3py. *J. Phys. Condens. Matter*, 35(35):353001, 2023.
  - [38] B.J. George and M.K. Alex. Possible high t c superconductivity in the ba-la-cu-o system. *Zeitschrift für Physik B Condensed Matter*, 64(2):189–193, 1986.
  - [39] G. Suyog, M. Blanka, N. Yoshio, and C.S. Krishna. Achieving direct band gap in germanium through integration of sn alloying and external strain. *Journal of Applied Physics*, 113(7), 2013.
  - [40] R. Yu, W. Zhang, H.J. Zhang, S.C. Zhang, and X. Dai and Z. Fang. Quantized anomalous hall effect in magnetic topological insulators. *science*, 329(5987):61–64, 2010.
  - [41] C.Z. Chang, J.S. Zhang, X. Feng, J. Shen, Z.C. Zhang, M.H. Guo, K. Li, Y.B. Ou, P. Wei, L.L. Wang, et al. Experimental observation of the quantum anomalous hall effect in a magnetic topological insulator. *Science*, 340(6129):167–170, 2013.
  - [42] R.N. Min, Y.X. Wang, X. Jiang, R.C. Chen, H.J. Kang, E. Y. Guo, Z.N. Chen, X. Yang, and T.M. Wang. Significantly improved thermoelectric properties of nb-doped zn1sn half-heusler compounds. *Chemical*

*Engineering Journal*, 449:137898, 2022.

- [43] Z.J. Lang, R.S. Jiang, and W. Ku. Strongly correlated doped hole carriers in the superconducting nickelates: their location, local many-body state, and low-energy effective hamiltonian. *Physical Review B*, 103(18):L180502, 2021.
- [44] C.H. Riedl, C. Coletti, T. Iwasaki, A.A. Zakharov, and U. Starke. Quasi-free-standing epitaxial graphene on sic obtained by hydrogen intercalation. *Physical review letters*, 103(24):246804, 2009.
- [45] C. Riedl, C. Coletti, and U. Starke. Structural and electronic properties of epitaxial graphene on sic (0 0 0 1): a review of growth, characterization, transfer doping and hydrogen intercalation. *Journal of Physics D: Applied Physics*, 43(37):374009, 2010.
- [46] S. Rajput, M.X. Chen, Y. Liu, Y.Y. Li, M. Weinert, and L. Li. Spatial fluctuations in barrier height at the graphene–silicon carbide schottky junction. *Nature communications*, 4(1):2752, 2013.
- [47] Y. Qi, S.H. Rhim, G.F. Sun, M. Weinert, and L. Li. Epitaxial graphene on sic (0001): more than just honeycombs. *Physical review letters*, 105(8):085502, 2010.
- [48] L. Li and I.S.T. Tsong. Atomic structures of 6h sic (0001) and (0001) surfaces. *Surface science*, 351(1-3):141–148, 1996.
- [49] K. Fukuma, A. Visikovskiy, T. Iimori, T. Miyamach, F. Komori, and S. Tanaka. Formation of graphene nanoribbons on the macrofacets of vicinal 6 h-sic (0001) surfaces. *Physical Review Materials*, 6(12):124003, 2022.
- [50] Z.C. Wang, S. Tsukimoto, M. Saito, and Y. Ikuhara. Sic/ti 3 sic 2 interface: Atomic structure, energetics, and bonding. *Physical Review B—Condensed Matter and Materials Physics*, 79(4):045318, 2009.
- [51] S.A. Meynell, A. Spitzig, B. Edwards, M.D. Robertson, D. Kalliecharan, L. Kreplak, and T.L. Monchesky. Structure of mnsi on sic (0001). *Physical Review B*, 94(18):184416, 2016.
- [52] A.P. Thompson, H.M. Aktulga, R. Berger, D.S. Bolintineanu, W.M. Brown, P.S. Crozier, Pieter J In't Veld, A. Kohlmeyer, S.G. Moore, T.D. Nguyen, et al. Lammmps—a flexible simulation tool for particle-based materials modeling at the atomic, meso, and continuum scales. *Computer Physics Communications*, 271:108171, 2022.
- [53] L. Bonati and M. Parrinello. Silicon liquid structure and crystal nucleation from ab initio deep metadynamics. *Physical review letters*, 121(26):265701, 2018.
- [54] L.F. Zhang, J.Q. Han, H. Wang, R. Car, and W.N. E. Deep potential molecular dynamics: a scalable model with the accuracy of quantum mechanics. *Physical review letters*, 120(14):143001, 2018.
- [55] H. Wang, L.F. Zhang, J.Q. Han, and W.N. E. Deepmd-kit: A deep learning package for many-body potential energy representation and molecular dynamics. *Computer Physics Communications*, 228:178–184, 2018.
- [56] Y.Z. Zhang, H.D. Wang, W.J. Chen, J.Z. Zeng, L.F. Zhang, H. Wang, and W.n. E. Dp-gen: A concurrent learning platform for the generation of reliable deep learning based potential energy models. *Computer Physics Communications*, 253:107206, 2020.
- [57] Y.X. Chen, L.F. Zhang, H. Wang, and W.N. E. Deepks: A comprehensive data-driven approach toward chemically accurate density functional theory. *Journal of Chemical Theory and Computation*, 17(1):170–181, 2020.
- [58] H. Li, Z. Wang, N.L. Zou, M. Ye, R.Z. Xu, X.X. Gong, W.H. Duan, and Y. Xu. Deep-learning density functional theory hamiltonian for efficient ab initio electronic-structure calculation. *Nature Computational Science*, 2(6):367–377, 2022.
- [59] H. Li, Z. Wang, N.L. Zou, M. Ye, R.Z. Xuand X.X. Gongand W.H. Duan, and Y. Xu. Deep-learning density functional theory hamiltonian for efficient ab initio electronic-structure calculation. *Nature Computational Science*, 2(6):367–377, 2022.